Order parameter measurements from the Kossel diagrams of the liquid-crystal blue phases

Richard J. Miller and Helen F. Gleeson*
Department of Physics and Astronomy, Schuster Laboratory, Manchester University, Manchester M13 9PL, United Kingdom
(Received 5 June 1995)

Scalar order parameter measurements of the liquid crystal blue phase II (BPII), taken using the Kossel diagram technique, are presented. The temperature dependence of the order parameter is found to follow a curve predicted by the Landau theory. The order parameter data, derived from the diffracted light intensity, are normalized such that the fitted theoretical temperature dependence has a value of unity at a temperature of 0 K, representing perfect order. This normalized order parameter is found to be approximately 0.1 within the blue phase. The theory of the temperature dependence of the blue phase order parameter is summarized, together with the measurement technique employed. The measurements were made possible by use of a high-resolution charge-coupled-device camera, frame grabber, and image-analysis computer software to capture the Kossel diagram images. Also, a high-stability temperature controller and reflection microscope were used.

PACS number(s): 61.30.Gd, 74.20.De, 42.25.Fx

I. INTRODUCTION

The blue phases [1] of liquid crystals are thermodynamically distinct phases which occur in materials with high chirality. They have been studied now for some years and the basic reasons for their existence are believed to be understood. However, techniques for measuring fundamental parameters, such as the order parameter and elastic constants, in these phases have not been significantly developed. Therefore, the aim of this paper is to examine the possibilities of measuring the order parameter in the blue phases using the Kossel diagram technique [2] which is discussed in some detail.

In work by previous authors [3] the order parameter in the blue phases has been determined, to within a common scaling factor, from the blue phase transmission spectra. The Kossel diagram technique, however, has only been exploited to determine the existence of crystal planes and overall symmetry in these phases. In this paper the salient points from the theory of the blue phases, which allow order parameter measurements to be made, are discussed. Then the Kossel diagrams of blue phase II (BPII) are used to give measurements of the order parameter, to within a common scaling factor, and these measurements normalized to give an absolute value of the order parameter.

II. THEORY

A. The order parameter in the periodic blue phases

In the nematic phase the order parameter is usually represented by a scalar parameter S, which takes a value between zero and 1 and quantifies the degree of ordering within the system. However, this order parameter is more correctly a second rank tensor [4] which also contains information about the spatial orientation of the molecules. In the more complex periodic blue phases the order parameter must also be represented by a second rank tensor which will generally be biaxial and periodic. The tensor order parameter may be represented by any of several different tensor properties of the liquid-crystal system as long as this tensor vanishes in the isotropic phase. Conventionally [5], in the periodic blue phases, the dielectric permittivity tensor $\varepsilon(\vec{r})$ is used since this may easily be related to the optical properties of the phases. The tensor order parameter is then defined by the anisotropic part of the dielectric permittivity tensor $\varepsilon^a(\vec{r})$, whose components are given by

$$\varepsilon^a_{ij}=\varepsilon_{ij}=\tfrac{1}{3}\,\mathrm{Tr}(\varepsilon)\delta_{ij}\ , \tag{1}$$

where $\mathrm{Tr}(\varepsilon)$ represents the trace of the tensor $\varepsilon(\vec{r})$.

Due to the periodicity of the blue phases the tensor order parameter $\varepsilon^a(\vec{r})$ may be expanded as a Fourier series in terms of the reciprocal lattice vectors $\vec{\tau}$, such that

$$\varepsilon^a(\vec{r})=\sum_{\vec{\tau}}\varepsilon^{\vec{\tau}}e^{i\vec{\tau}\cdot\vec{r}}\ , \tag{2}$$

where $\varepsilon^{\vec{\tau}}$ is the tensor Fourier component. This expansion is found to be particularly useful when considering the light scattering properties of the blue phases.

B. The Landau theory of blue phases

The theoretical description of the blue phases within the framework of the Landau theory [6] of phase transitions has been highly successful in predicting the existence of the blue phases. In particular, this theory was developed by Brazovskii and co-workers [7] and Hornreich and Shtrikman [8] (see also the reviews [9]). As in all Landau phase transition theories it concentrates on the symmetry properties, as described by an order parameter, of two phases either side of a phase transition.

*Corresponding author.

Then the free energy of the system is expanded as a series in the lowest powers of the order parameter allowed by symmetry. Finally, the free energy is minimized in order to obtain the equilibrium phase structure.

Due to the complexity of the blue phase system the free energy must be minimized numerically with a limited number of reciprocal lattice vector Fourier components. In this way the theoretically determined phases have been found to be in close agreement with those observed experimentally [10]. These numerical calculations have revealed two remarkable properties of the blue phase structures [3]. First, a few of the Fourier components $\vec{\varepsilon^{\tau}}$ of the order parameter are found to be much larger than the others. Second, the relative magnitudes of these components turn out to be virtually independent of the temperature and other parameters in the free energy equation. These properties, confirmed by experiment [11], allow the theoretical description of the blue phases to be greatly simplified by the extraction of a scalar quantity ε_S containing the temperature dependence of the phases. Also only a few of the Fourier components are needed to describe the phases. Hence

$$\vec{\varepsilon^{\tau}}=\varepsilon_S \vec{\mathbf{U}^{\tau}}\,, \tag{3}$$

where the tensor $\vec{\mathbf{U}^{\tau}}$ contains only the structural information of the Fourier component. In this simplified theory the temperature dependence of what may be called the scalar order parameter ε_S takes the form [3]

$$\varepsilon_S=\alpha\left[1+\sqrt{\tfrac{1}{9}+\beta(T_C-T)}\right], \tag{4}$$

where α and β are constants, T is the temperature in K, and T_C is the temperature of the transition from blue phase to isotropic phase in K.

C. Light scattering in the blue phases and measurement of the order parameter

The kinematic theory of light scattering in the blue phases is the simplest treatment due to various simplifying assumptions. It neglects multiple scattering and attenuation of the incident beam and hence applies to thin samples in which the intensity of the scattered beam is much less than that of the incident beam. In this theory the coefficient of reflection from a thin single crystal, with reciprocal lattice vector $\vec{\tau}$, is given by [12]

$$R(\vec{e}_0,\vec{e}_d)\equiv\frac{I_d}{I_0}=|\vec{e}_d^{\,*}\vec{\varepsilon^{\tau}}\vec{e}_0|^2 R_{\vec{\tau}}\,, \tag{5}$$

where I_0 is the intensity of the incident wave with polarization unit vector $\vec{e}_0$, I_d is the intensity of the diffracted wave with polarization unit vector $\vec{e}_d$, $|\vec{e}_d^{\,*}\vec{\varepsilon^{\tau}}\vec{e}_0|^2$ is a polarizational-structural factor, and $\vec{\varepsilon^{\tau}}$ is a Fourier component of the order-parameter tensor, as above. The factor $R_{\vec{\tau}}$ contains the geometry of the system and varies according to the directions of the incident and diffracted radiation, reaching a maximum when the Bragg condition is satisfied.

Using the theory discussed in the previous section the Fourier component $\vec{\varepsilon^{\tau}}$ may be replaced by $\varepsilon_S\vec{\mathbf{U}^{\tau}}$ and the factor ε_S taken out such that the reflection coefficient is now given by

$$R(\vec{e}_0,\vec{e}_d)\equiv\frac{I_d}{I_0}=\varepsilon_S^2|\vec{e}_d^{\,*}\vec{\mathbf{U}^{\tau}}\vec{e}_0|^2 R_{\vec{\tau}}\,. \tag{6}$$

This equation, however, only considers plane parallel incident light. The situation becomes more complex in the case of Kossel diagrams where light converges on the crystal from many directions. Hence light diffracted in a particular direction contains contributions from a broad range of incident angles. Most of these contributions come from the small range of angles close to the Bragg condition. Hence, neglecting interference, the intensity of light diffracted in a particular direction is given by

$$I_d=\varepsilon_S^2 I_0\int|\vec{e}_d^{\,*}\vec{\mathbf{U}^{\tau}}\vec{e}_0|^2 R_{\vec{\tau}}\,d\sigma\,, \tag{7}$$

where the integral is taken over the solid angle. Assuming that the reciprocal lattice vector and the refractive index of the sample do not change with temperature, the integral is just a structural factor. Then the temperature dependence of the equation is all contained within the scalar order parameter ε_S. Hence, with the proviso that all other experimental conditions remain the same, it is possible to determine the scalar order parameter to within a common scaling factor by measuring the variation in the scattered light intensity with temperature. It is found experimentally that the refractive index is virtually constant over the temperature range of the blue phases [13]. However, in general it is found that the magnitude of the reciprocal lattice vectors may vary by 5% over the range of the phase [14]. Hence the integral in Eq. (7) is not completely independent of temperature but its value will vary on the order of 5% due to changes in the reciprocal lattice vector.

III. EXPERIMENTAL METHOD

A. The Kossel diagram technique

Kossel diagrams are one of the experimental techniques which have been used in recent years for studying the periodic blue phases. The Kossel diagram technique [15] was first developed in 1935 for the study of crystal structures using x rays. However, it may also be applied to chiral structures in liquid crystals where the periodicities are of the same order as visible wavelengths.

The technique uses monochromatic light such that the blue phase sample is flooded with a highly convergent beam. Some of this incident light, interacting with lattice planes within the sample, will then fulfill the Bragg condition and be diffracted while light from other directions will pass unhindered through the sample (Fig. 1). This diffracted light will form part of a cone of light diffracted from a set of planes in the sample whose axis is the reciprocal lattice vector of the planes and whose cone angle is given by the Bragg condition.

The most convenient way to provide highly convergent light for the small sample size typically used for liquid crystals is via a microscope objective. The objective then collects the cone of diffracted light which comes to focus

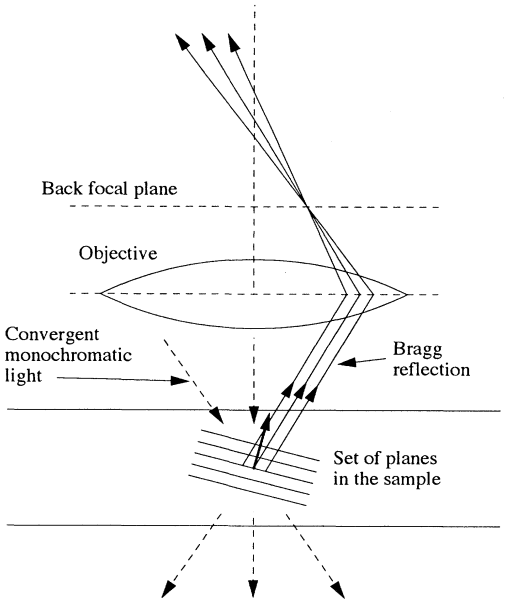

FIG. 1. Schematic diagram illustrating the Kossel diagram technique. The Kossel diagram is generated in the back focal plane by the focusing of parallel light reflected from the sample.

in the back focal plane of the objective. Here it produces a circle, ellipse, or line depending upon the relative orientation of the cone axis. Since the incident convergent light will, in general, fulfill the Bragg condition for more than one set of planes in the sample, the back focal plane image consists of sets of circles, ellipses, and lines. Their dimensions depend directly on the wavelength of the incident light and the orientation and size of the reciprocal lattice vectors in the sample. Such an image is called a Kossel diagram.

In order to achieve as large a range of incident angles of light as possible it is necessary to choose an objective for the microscope with a large numerical aperture N. Via Snell's law this relates directly to the largest angle α of convergent light in the sample relative to the central axis of the optics, such that

$$N = n \sin\alpha \ , \tag{8}$$

where n is the refractive index of the sample. Liquid crystals typically have a refractive index of the order of 1.6. Hence, using a 100× oil immersion objective with a large numerical aperture of 1.3 gives a maximum cone angle inside the liquid crystal of about 55°.

B. The Kossel diagram apparatus

As discussed above, Kossel diagrams are viewed in the back focal plane of the objective when the sample is illuminated with monochromatic light. In these experiments an Ion Laser Technology 450ASL tunable argon ion laser was used as a light source. This was coupled to the reflection arm of an Olympus BHMJ metallurgical reflection microscope using a short length of fiber optic bundle. The laser exhibited two strong emissions at 514.5 and 488.0 nm as well as weaker radiation at wavelengths including 476.5 and 457.9 nm. The power output in the strong lines could be varied from 3 to 20 mW. The wavelengths produced by the argon ion laser are ideally suited to viewing the blue-phase Kossel lines since they are at the short end of the visible wavelength range. A speckle pattern, due to the coherence of the laser light, was superimposed on the Kossel image, but was effectively removed by vibrating the fiber optic bundle with a small speaker, powered by a signal generator. The fiber optic cable gave the added advantages of depolarizing the light and allowing easy coupling of the light source to the microscope reflection arm.

A Bertrand lens, normally used to obtain an image of the back focal plane, was not available for this microscope. Hence it was necessary to construct equipment which would image the back focal plane in the video camera used to record the image. This Kossel diagram imager was designed to replace the trinocular head and fixed analyzer of the microscope. At the bottom of the imager is a base which both holds a polarizer and attaches to the microscope. Above this, three 35 cm steel posts support the charge-coupled-device (CCD) camera situated at the center of a metal plate. The camera used was a Hitachi Denshi KP-M1 black and white CCD camera since this is small and light but at the same time gives a high resolution of 640×480 pixels. A second plate holding a simple biconvex lens is free to move along the steel posts on bearings and its position is controlled by a long steel rod taped with a screw thread. The focusing of the camera is then controlled by simply turning the tapped steel rod. An aperture of about 1 cm diameter was placed in front of this lens to help cut out stray light from the image.

An Olympus 100× oil immersion objective ($N=1.3$) was used to take the Kossel diagram images. The use of an oil immersion lens requires placing the objective in thermal contact with the sample. As the blue phases are temperature sensitive, and exist over only $\sim 1\,^{\circ}\mathrm{C}$, it was necessary to minimize the thermal gradient between the objective and the sample. The temperature of the microscope objective was matched to that of the sample using a brass heating collar which was controlled, independently of the sample temperature, with a Linkam TMS90 temperature controller. The Linkam temperature controller gave a temperature stability of 0.01 °C. The objective was insulated from the microscope body by a thin steel extension tube. The Linkam controller was calibrated against the sample heating stage via a sample phase transition. The temperature gradient across the sample could then be held to within 0.04 °C. The sample heating stage itself has been described in detail elsewhere [16] and has a temperature stability within 0.01 °C.

C. Data capture and analysis

Video pictures of the Kossel diagrams, taken by the CCD camera, were digitized using a DIPIX Technologies P360F frame grabber [17] and image processing software [18] both installed onto a 486 IBM compatible personal computer. The digitized pictures produced have a resolution of 640×480 pixels. The software allows many im-

ages of the Kossel diagrams to be taken and averaged to reduce noise and also allows direct access to the light intensity information contained within the images. The images could also be processed to improve their contrast and brightness in order to emphasize certain features in the diagrams.

The Kossel diagram images were processed using the image analysis software to obtain the order-parameter information. A cross section of the light intensity across one of the Kossel lines was taken and a Gaussian curve combined with a linear baseline (to allow for the background light intensity) were fitted to the data. Using the same cross section across the same Kossel line the temperature of the sample was varied, allowing the temperature dependence of the Kossel line intensity to be determined.

IV. MATERIALS

The material used was chosen because it exhibits both of the cubic blue phases (BPI and BPII) with reasonably useful temperature range ($\sim 1\,^{\circ}C$), selective reflection in the visible light wavelength range, and at a convenient temperature ($\sim 45\,^{\circ}C$). It consisted of 20.1 ± 0.2 mol % of 4''-(2-methyl)butylphenyl-4'-(2-methyl)butyl-4-biphenyl carboxylate (CE2) in 4-cyano-4'-*n*-butylbiphenyl (4CB). Both of these components were provided by Merck U.K. Ltd. [19] and their naming convention has been used. The chemical structures of the compounds are shown in Fig. 2. The phase transition temperatures of the mixture were found using the high stability temperature controller to be $47.18\,^{\circ}C$ for the cholesteric to BPI transition, $47.47\,^{\circ}C$ for the BPI to BPII transition, $48.12\,^{\circ}C$ for a transition to a BPII-isotropic biphasic region, and with the clearing point at $48.24\,^{\circ}C$. These measurements were made with an accuracy of $\pm 0.01\,^{\circ}C$. The material was contained in a thin cell (spacing $\sim 10\ \mu m$) formed by two pieces of glass, domain regions of the sample were generally easy to obtain in BPII. However, as commonly found, BPI tended to form much smaller domains.

V. RESULTS AND DISCUSSION

Kossel diagram images were taken at a range of different temperatures across BPII of the mixture of CE2 and 4CB discussed above. The wavelength of the argon ion laser was tuned to 514.5 nm. Figure 3 shows typical

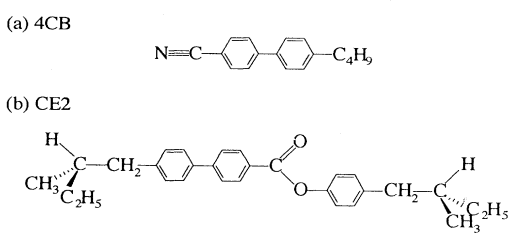

FIG. 2. Chemical structures of the compounds used in the mixture for this paper. These compounds were provided by Merck U.K. Ltd.

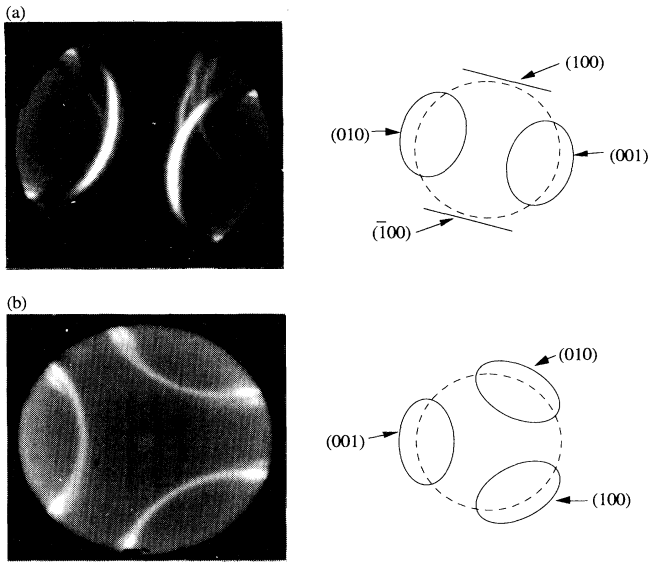

FIG. 3. Two Kossel diagram images taken in BPII, $0.10\,^{\circ}C$ below the BPII to isotropic phase transition at 514.5 nm, for different crystal orientations. (a) [011] viewing direction. (b) [111] viewing direction. The theoretical Kossel diagrams shown, corresponding approximately to the images, are to aid identification of the different lines. The dashed circle in the schematic diagrams shows the limit of the field of view in the images.

Kossel images taken within BPII at $48.02\,^{\circ}C$. Each image shows a different crystal orientation, identified with the aid of theoretical Kossel diagrams [20]. Figure 3(a) shows Kossel diagrams taken from BPII with the viewing direction along [011], showing the (010) and (001) lines, while Fig. 3(b) is along the [111] direction, showing these same lines plus (100). The theoretical Kossel digrams for approximately equal lattice parameters are shown alongside the images in each of the figures, picking out the reciprocal lattice vectors associated with each line. These images are of comparable quality to those found in other work [21].

As discussed above (Sec. II C) the integral in Eq. (7) is not completely free of temperature dependence but varies with changes in the reciprocal lattice vector. Figure 4 shows measurements of the helical pitch across BPI and BPII made in parallel with this work [14]. The data show that in this mixture the reciprocal lattice vectors varied by no more than about 3% across BPII. Consequently, measurements of the order parameter may be made to within a common scaling factor and an error of 3%.

The order parameter measurements were obtained using the (001) Kossel line in BPII viewed along the [111] direction, throughout the BPII temperature range. The intensity profiles were measured along a radial line, perpendicular to the Kossel line. The height of the Gaussian fit to the Kossel line profile above the baseline was then taken as proportional to the intensity of the Kossel line, I_d, and the square root of this as proportional to the blue phase scalar order parameter ε_S. The BPI Kossel diagram images taken were found to be too noisy for accu-

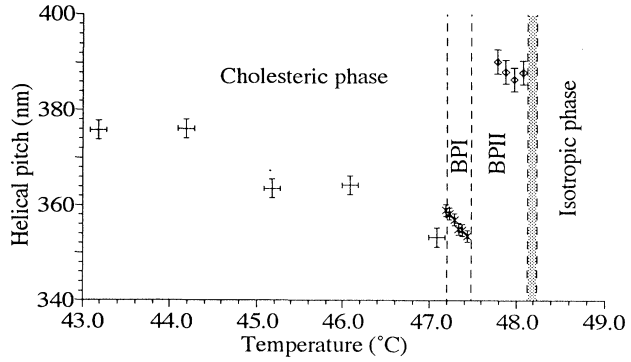

FIG. 4. The pitch measured in the cholesteric phase and blue phases as a function of temperature. In each of the blue phases the pitch, and hence reciprocal lattice vectors, change by no more than 3%. The discrete steps in the changing cholesteric pitch are due to the planar cell alignment pinning the molecules at the glass and liquid crystal interfaces.

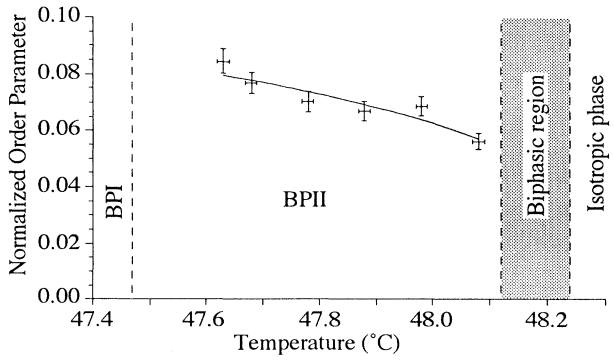

FIG. 5. Normalized order parameter taken from the (001) Kossel line in BPII. These data are normalized such that the fit of the theoretical curve has a value of unity at 0 K.

rate analysis, causing problems in determining a baseline for the Gaussian curve. This was possibly due to the larger number of Kossel lines which are generally obtained in BPI plus the fact that BPI tends to form smaller crystal domains than BPII and hence was less well aligned.

In the theory section above (Sec. II B) the temperature dependence of the blue phase scalar order parameter ε_S, derived from Landau theory, was given as

$$\varepsilon_S = \alpha\left[1+\sqrt{\tfrac{1}{9}+\beta(T_C-T)}\right]$$

[Eq. (4)], where α and β are constants, T is the temperature, and T_C is the temperature of the blue phase to isotropic liquid phase transition. A fit of Eq. (4) was then made to the order-parameter data. For this fit the blue phase to isotropic phase transition, T_C, was taken as the lower limit of the biphasic region. The fit of the theoretical curve was then used to scale the original order-parameter data such that the fitted curve has a value of unity at 0 K, representing perfect order. The normalized order-parameter data are shown in Fig. 5, along with the fitted theoretical curve. It can be seen that the normalized order parameter within BPII is approximately 0.1 which, although low, is perfectly reasonable. Given the errors shown in this graph and the relatively small number of data points near T_C, the fit employed is by no means unique, but does have a sound theoretical basis. This normalized order parameter is arguably equivalent to the order parameter commonly used in the nematic phases.

VI. CONCLUSIONS

In this paper quantitative order parameter measurements have been taken from the Kossel diagrams of BPII. The measurements were made possible by noting that the magnitude of the anisotropic part of the dielectric permittivity tensor, commonly used as the order parameter in the blue phases, may be directly related to the intensity of the Kossel lines. A high resolution system for generating Kossel diagram images has been constructed. This system, by virtue of the use of a laser and computer based image analysis, has generated high quality images, allowing quantitative measurements of the Kossel lines to be made. The blue phase order parameter was found to decrease with increasing temperature, as predicted by Landau theory. The normalized order parameter in BPII is found to have a value of about 0.1. Similar measurements have been made previously from the transmission spectra of the blue phases in different mixtures, but not related to a normalized order parameter. Using the Kossel diagram technique allows a specific, monodomain region of the blue phase to be selected for study and the data acquisition technique is both rapid and accurate.

ACKNOWLEDGMENTS

The authors would like to thank the SERC (now EPSRC) for provision of funding during the course of this work (R.J.M.) and the Royal Society for an equipment grant for the CCD camera and frame grabber.

[1] P. P. Crooker, Liq. Cryst. **5**, 751 (1989); H. Stegemeyer *et al.*, *ibid.* **1**, 3 (1986); V. A. Belyakov and V. E. Dmitrienko, Usp. Fiz. Nauk **146**, 369 (1985) [Sov. Phys. Usp. **28**, 535 (1985)].

[2] P. E. Cladis, T. Garel, and P. Pieranski, Phys. Rev. Lett. **57**, 2841 (1986); B. Jérôme and P. Pieranski, Liq. Cryst. **5**, 799 (1989); G. Heppke *et al.*, J. Phys. (Paris) **50**, 549 (1989).

[3] V. A. Belyakov *et al.*, Zh. Eksp. Teor. Fiz. **89**, 2035 (1985) [Sov. Phys. JETP **62**, 1173 (1985)].

[4] P. G. De Gennes and J. Prost, *The Physics of Liquid Crystals,* 2nd ed. (Clarendon, Oxford, 1993), p. 56.

[5] R. M. Hornreich and S. Shtrikman, Mol. Cryst. Liq. Cryst. **165**, 183 (1988).

[6] L. D. Landau and E. M. Lifshitz, *Statistical Physics,* 1st ed. (Pergamon, London, 1959), Chap. 14; C. Kittel and H.

Kroemer, *Thermal physics*, 2nd ed. (Freeman, San Francisco, 1980), p. 298.
[7] S. A. Brazovskii and S. G. Dmitriev, Zh. Eksp. Teor. Fiz. **69**, 979 (1976) [Sov. Phys. JETP **42**, 497 (1976)]; S. A. Brazovskii and V. M. Filev, *ibid.* **75**, 1140 (1979) [*ibid.* **48**, 573 (1979)].
[8] R. M. Hornreich and S. Shtrikman, Phys. Rev. A **24**, 635 (1981); **28**, 1791 (1983); **30**, 3264 (1984).
[9] P. P. Crooker, Mol. Cryst. Liq.. Cryst. **98**, 31 (1983); V. A. Belyakov and V. E. Dmitrienko, Usp. Fiz. Nauk **146**, 369 (1985) [Sov. Phys. Usp. **28**, 535 (1985)]; R. M. Hornreich and S. Shtrikman, Mol. Cryst. Liq. Cryst. **165**, 183 (1988).
[10] H. Grebel, R. M. Hornreich, and S. Shtrikman, Phys. Rev. A **30**, 3264 (1984); R. M. Hornreich and S. Shtrikman, *ibid.* **24**, 635 (1981).
[11] V. A. Kizel and V. V. Prokorov, Pis'ma Zh. Eksp. Teor. Fiz. **38**, 283 (1983) [JETP Lett. **38**, 337 (1983)]; Zh. Eksp. Teor. Fiz. **87**, 450 (1984) [Sov. Phys. JETP **60**, 257 (1984)].
[12] V. A. Belyakov *et al.*, Zh. Eksp. Teor. Fiz. **83**, 585 (1982) [Sov. Phys. JETP **56**, 322 (1982)]; V. A. Belyakov and V. E. Dmitrienko, Usp. Fiz. Nauk **146**, 369 (1985) [Sov. Phys. Usp. **28**, 535 (1985)]; Nuovo Cimento D **10**, 1293 (1988).
[13] K. Bergmann and H. Stegemeyer, Ber. Bunsenges. Phys. Chem. **82**, 1309 (1978).
[14] R. J. Miller, Ph.D. thesis, University of Manchester, England, 1994.
[15] W. Kossel, V. Loeck, and H. Voges, Z. Phys. **94**, 139 (1935).
[16] R. J. Miller and H. F. Gleeson, Meas. Sci. Technol. **5**, 904 (1994).
[17] DIPIX Technologies Inc., 1050 Baxter Rd., Ottawa, Ontario, Canada.
[18] ACCUWARE version 2.4, Automated Visual Inspection, 2519 Palmdale Court, Santa Clara, CA 95051.
[19] Merck U.K. Ltd., Merck House, Poole, Dorset, U.K.
[20] H.-S. Kitzerow, Ph.D. thesis, University of Berlin, Germany, 1989.
[21] B. Jérôme and P. Pieranski, Liq. Cryst. **5**, 799 (1989).

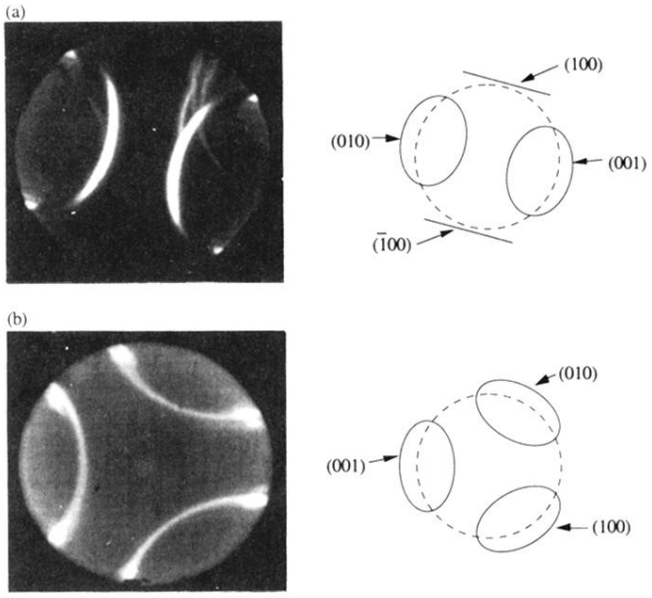

FIG. 3. Two Kossel diagram images taken in BPII, 0.10°C below the BPII to isotropic phase transition at 514.5 nm, for different crystal orientations. (a) [011] viewing direction. (b) [111] viewing direction. The theoretical Kossel diagrams shown, corresponding approximately to the images, are to aid identification of the different lines. The dashed circle in the schematic diagrams shows the limit of the field of view in the images.